JACS
JOURNAL OF THE AMERICAN CHEMICAL SOCIETY

ARTICLE

pubs.acs.org/JACS

Probing Conformational Variations at the ATPase Site of the RNA Helicase DbpA by High-Field Electron−Nuclear Double Resonance Spectroscopy

Ilia Kaminker,[†] Anastasiya Sushenko,[†] Alexey Potapov,[†] Shirley Daube,[‡] Barak Akabayov,[§] Irit Sagi,[§] and Daniella Goldfarb*[,†]

[†]Department of Chemical Physics, [‡]Department of Chemical Infrastructure, and [§]Department of Structural Biology, Weizmann Institute of Science, Rehovot 76100, Israel

Supporting Information

ABSTRACT: The RNA helicase DbpA promotes RNA remodeling coupled to ATP hydrolysis. It is unique because of its specificity to hairpin 92 of 23S rRNA (HP92). Although DbpA kinetic pathways leading to ATP hydrolysis and RNA unwinding have been recently elucidated, the molecular (atomic) basis for the coupling of ATP hydrolysis to RNA remodeling remains unclear. This is, in part, due to the lack of detailed structural information on the ATPase site in the presence and absence of RNA in solution. We used high-field pulse ENDOR (electron−nuclear double resonance) spectroscopy to detect and analyze fine conformational changes in the protein's ATPase site in solution. Specifically, we substituted the essential Mg^{2+} cofactor in the ATPase active site for paramagnetic Mn^{2+} and determined its close environment with different nucleotides (ADP, ATP, and the ATP analogues ATPγS and AMPPnP) in complex with single- and double-stranded RNA. We monitored the Mn^{2+} interactions with the nucleotide phosphates through the ^{31}P hyperfine couplings and the coordination by protein residues through ^{13}C hyperfine coupling from ^{13}C-enriched DbpA. We observed that the nucleotide binding site of DbpA adopts different conformational states upon binding of different nucleotides. The ENDOR spectra revealed a clear distinction between hydrolyzable and nonhydrolyzable nucleotides prior to RNA binding. Furthermore, both the ^{13}C and the ^{31}P ENDOR spectra were found to be highly sensitive to changes in the local environment of the Mn^{2+} ion induced by the hydrolysis. More specifically, ATPγS was efficiently hydrolyzed upon binding of RNA, similar to ATP. Importantly, the Mn^{2+} cofactor remains bound to a single protein side chain and to one or two nucleotide phosphates in all complexes, whereas the remaining metal coordination positions are occupied by water. The conformational changes in the protein's ATPase active site associated with the different DbpA states occur in remote coordination shells of the Mn^{2+} ion. Finally, a competitive Mn^{2+} binding site was found for single-stranded RNA construct.

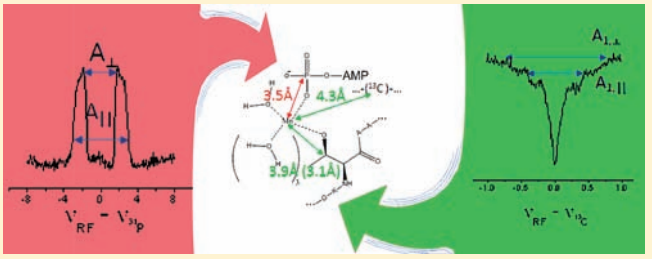

INTRODUCTION

DEAD-box protein A (DbpA) is one of five *Escherichia coli* DEAD-box helicases.[1] Helicases bind and remodel nucleic acids or nucleic acid−protein complexes in an ATP-dependent manner.[2] They are encoded by virtually all organisms from viruses and bacteria to humans and constitute one of the largest classes of proteins.[3] DEAD-box helicases are part of superfamily 2 (SF2).[4] The name of this family is derived from the conserved DEAD motif (Asp Glu Ala Asp), also known as Walker B motif.[5] Members of the DEAD-box RNA helicase family were found to participate in a variety of biological processes such as translation initiation, ribosome biogenesis, RNA splicing, microRNA function, RNA transport, viral RNA replication, and many other process that were recently reviewed.[6,7] DbpA was proposed to take part in ribosome biogenesis, but to date its biological function is unclear.[1,8] DEAD-box helicases form a unique family of nonprocessive helicases within SF2. Nonprocessive helicases do not translocate along long duplexes of nucleic acids and unwind them; instead, they are thought to unwind and remodel short RNA structures at specific key positions.[2] They consist of two well-conserved RecA-like domains, with up to 13 characterized conserved motifs, which are essential for their basic functions such as RNA helix disruption and ATP hydrolysis.[4,9] Additional N or C terminal auxiliary domains confer the specific function to each of the helicases.

DbpA from *Escherichia coli* and its *Bacillus subtilis* homologue, YxiN, are unique among the DEAD proteins because their ATPase activity is strongly enhanced by the presence of an RNA molecule that contains the hairpin 92 of 23S rRNA (HP92) with either 3′ or 5′ extensions.[10−12] DbpA was shown to unwind short <9bp (base pairs) RNA duplexes positioned 3′ or 5′ to the HP92[13] as well as long duplex RNA stretches[14] in an ATP-dependent manner. Despite some recent progress in the field,[9] including

Received: May 10, 2011
Published: August 08, 2011

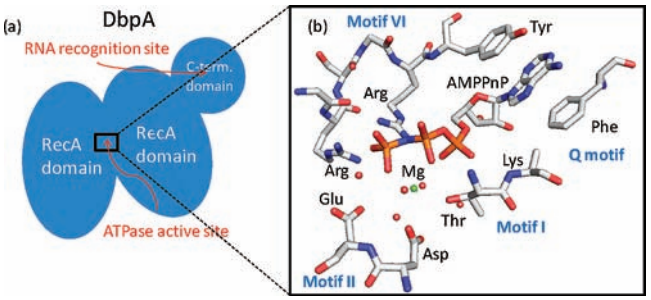

Figure 1. (a) Schematic representation of the relative positions of the three DbpA domains showing the ATPase and RNA recognition sites. (b) Atomic resolution structure of the DEAD-box helicase Mg^{2+} binding site. The presented structure is based on the crystal structure of eIF4AIII, in the Exon Junction complex, PDB accession code 2HYI.[24]

detailed elucidation of the DbpA kinetic pathway leading to ATP hydrolysis and RNA unwinding,[15] the fine molecular and chemical mechanisms associated with the different states DbpA adopts during the catalytic cycle are not yet fully understood.

The structure of the DbpA/RNA/nucleotide complex has not yet been determined. Homology modeling and biochemical data suggest that it consists of the helicase core formed by two RecA domains and an additional C-terminus domain that confers its specificity to the HP92 of the 23S rRNA.[16−18] A structural model (see the scheme in Figure 1a) of the homologous YxiN, which includes all three domains, has been recently proposed on the basis of SAXS (small-angle X-ray scattering)[19] and FRET (Forster energy transfer)[20] measurements. DbpA is known to adopt different conformations upon binding of ADP, ATPγS, and RNA.[21] YxiN exhibits a closed conformation, with the two RecA domains in proximity upon simultaneous binding of AMPPnP and RNA.[22] This closed conformation, with the two RecA domains forming a common interface, was observed in the crystal structures of the homologous DEAD-box proteins, Vasa, eIF4AIII, Mss116p, DDX19 cocrystallized with AMPPnP, and short polyU RNA fragments.[23−26] The nucleotide binding site is formed at the interface between the two RecA domains. Amino acids from the Walker A and Walker B (DEAD-box) motifs (N-terminal RecA domain) and motif VI (C-terminal RecA domain) interact with the bound nucleotide and are involved in ATP hydrolysis either directly or through structural water and an essential Mg^{2+} cofactor. The precise roles of the different conserved amino acids are difficult to elucidate. On the basis of crystal structures and biochemical data available for homologous DEAD-box proteins,[27,28] the following has been proposed: a conserved glutamate (Glu154 in DbpA sequence) of the DEAD motif activates the catalytic water molecule that attacks the γ phosphoryl group of ATP. The two conserved arginine residues (Arg331, Arg334 in the DbpA sequence) from motif VI interact directly with the γ phosphoryl group through H-bonds and are thought to function as a sensor for ATP versus ADP discrimination in a manner similar to arginine finger, first identified in Ras.[29] The Q motif positioned upstream to the Walker A motif confers specificity toward the ATP nucleotide through stacking interactions with the adenine base.[7,9] The direct coordination environment of the Mg^{2+} ion varies in different crystal structures of DEAD-box RNA helicases; the observed coordination schemes are summarized in Table S1. In general, it is coordinated to two nucleotide phosphates, one or two oxygen atoms belonging to the carboxyl or hydroxyl groups of the protein residues and water molecules. A representative structure of the DEAD helicase ATP binding site of eIF4AIII is presented in Figure 1b.

The mechanistic aspects of the coupling between ATP hydrolysis and RNA remodeling in DbpA is a key issue that is still unresolved. Its understanding requires atomic-level structural information about the ATPase active site because small changes in the active site are expected to start the cascade of events, which eventually leads to RNA helix disruption and remodeling. Magnetic resonance spectroscopic techniques, known to effectively provide structural information in solution, have not yet been applied to RNA helicases. In this work, we explored the structure of the ATPase site of DbpA by high-field (W-band, 95 GHz) pulse electron−nuclear double resonance (ENDOR) spectroscopy, using the essential divalent cation cofactor in the ATPase active site as a probe. We substituted the Mg^{2+} cofactor for the EPR active ion Mn^{2+} ($S = 5/2$; $I = 5/2$). Mn^{2+} is a common substitute for Mg^{2+} because of their similar properties,[30,31] and DbpA retains its ATPase activity upon this substitution.[32] We probed the local environment of Mn^{2+} in the DbpA ATPase active with different ATP analogues and RNA substrates. High-field measurements are highly advantageous because of their high sensitivity to Mn^{2+} and the simplicity of its EPR spectrum, and their high resolution in terms of the ENDOR frequencies.[33]

We found that the binding of different nucleotides and RNA substrates resulted in distinct and highly reproducible ENDOR spectra. The spectral changes were specifically correlated with the binding of ADP, ATP, and the ATP analogues ATPγS and AMPPnP, which resulted in local changes in metal−cofactor coordination and metal protein interactions. In all of the investigated protein states, the Mn^{2+} cofactor remained bound to a single protein side chain of DbpA, whereas other metal coordination positions were occupied by the nucleotide phosphates and water molecules. Upon binding of RNA, structural changes in the protein occur beyond the first coordination shell of the Mn^{2+} ion. The ENDOR spectra were highly sensitive to ATP hydrolysis upon RNA binding and showed that ATPγS is also efficiently hydrolyzed. Finally, using ENDOR spectroscopy, we could also detect the formation of a Mn^{2+} binding site in the 5′ extension of the single-stranded RNA, the affinity of which was comparable to that of the enzyme ATPase site.

EXPERIMENTAL SECTION

Protein Preparation. DbpA protein was overexpressed and purified as described previously.[14] Briefly, the *E. coli* strain BL21 (DE3) pLysS cells containing the DbpA vector were grown in M9-ZB medium at 37 °C. Overexpression was induced with 0.2 mM isopropyl β-D-thiogalactopyranoside at A_{600} = 0.5, and the cells were grown at 30 °C with vigorous shaking for ∼12 h. The cell pellet was collected by centrifugation and resuspended in a 20 mM MOPS, pH 6.8/250 mM NaCl/1 mM DTT/protease inhibitor mixture (Complete mini EDTA-free, Roche) and then sonicated on ice. Cell debris was removed by centrifugation, and the supernatant was diluted to a final buffer concentration of 20 mM MOPS, pH 6.8/100 mM NaCl and loaded onto a DEAE column equilibrated with 20 mM MOPS, pH 6.8/100 mM NaCl/1 mM DTT/1 mM PMSF/1 mM benzamidine. The flowthrough was then loaded onto an SP column equilibrated with the same buffer and eluted with a linear gradient of 0.1−1 M NaCl. The relevant protein fractions were pooled together and loaded onto a gel filtration HiLoad 16/26 Superdex 75 prep grade column equilibrated with 20 mM HEPES, 200 mM NaCl, pH 7.5. The clean fractions were combined to provide the final protein sample. Protein purity was estimated to be

above 90% based on SDS PAGE, and protein concentration was estimated by optical absorption at 280 nm using an extinction coefficient of ε = 25 200 $cm^{-1}\,M^{-1}$. The ATPase activity of the protein was measured with the commercially available EnzChek Phosphate Assay Kit (Molecular Probes Invitrogen). The protein was concentrated to ~0.2−0.7 mM in 50% glycerol using Vivaspin concentrators (Sartorius) and stored at −80 °C until use.

Uniformly ^{13}C-labeled DbpA was overexpressed in the M9 minimal media with the ^{13}C -labeled D-glucose (Cambridge Isotopes) as the only carbon source and purified as the natural abundance protein. The extent of ^{13}C labeling was confirmed by mass spectrometry to be ~95%. The ATPase activity of the ^{13}C-labeled protein was within the usual batch-to-batch difference for unlabeled DbpA protein purification as measured by an ATPase activity assay.

RNA Preparation. All RNA constructs were purchased from Dharmacon, deprotected as instructed, purified by cutting a single band from the denaturating polyacrylamide gel, extracted with phenol, precipitated with 70% ethanol, dried using a SpeedVac, and then stored as dry powder at −20 °C until use.

EPR Sample Preparation. RNA constructs were dissolved in RNA folding buffer (50 mM HEPES, 100 mM NaCl, 30% (v/v) glycerol, pH 7.5) and folded by gradually cooling from 95 °C to room temperature. Folded RNA was mixed with an equimolar amount of nucleotide (ADP, AMPPnP, ATPγS)/Mn^{2+} solution and a slight excess of DbpA. The ADP and AMPPnP nucleotides were purchased from Sigma Aldrich and the ATPγS from Merck Biosciences. The final composition of the samples was nucleotide/RNA/Mn^{2+} ratios of 1:1:1 and a slight excess of the protein (~10−30%). The final concentration varied from ~0.075 to 0.15 mM, depending on the batch of protein and RNA used. The sample was thoroughly mixed by pipetation, loaded into W-band EPR tubes (i.d. 0.64 mm, o.d. 0.8 mm), frozen in liquid nitrogen, and finally stored in liquid nitrogen until measured. All ENDOR samples, except those prepared with ATP nucleotides that were prepared only once, were prepared and measured two or more times using independent RNA/DbpA preparations for all types of samples.

The binding constants for nucleotide analogues and RNA are well-known for DbpA[15] (see Table S1 in ref 15). They were determined for Mg^{2+}, and we assumed that they are not much different for Mn^{2+}. On the basis of these binding constants, the binding of RNA to the protein is rather strong and will result in ~90−95% complex formation, whereas the addition of Mn^{2+}/nucleotide will result in ~75% and ~50% complex formation for tertiary complexes with the ADP and ATP analogues, respectively. This means that a significant amount of the free Mn^{2+}/ADP (or ATP analogues) is present in solution. To reduce the amount of free Mn^{2+}/nucleotide, we could in principle reduce the Mn^{2+} concentration further, but this was not possible due to S/N considerations because Mn^{2+} is used as a probe in our experiments. Alternatively, the DbpA concentration could be increased, but here we faced problems due to limited solubility. RNA binding to DbpA requires precisely folded RNA molecules. The presence of the misfolded RNAs will result in less complex formation than was previously calculated.

EPR and ENDOR Spectroscopy. The frozen EPR samples were loaded into the EPR probehead while immersed in a liquid N_2 bath, and then the entire cold probe was transferred to the precooled cryostat.

All spectra were acquired on a home-built W-band EPR spectrometer.[34,35] Echo-detected EPR spectra were recorded using a $\pi/2-\tau-\pi-\tau-$echo pulse sequence by varying the magnetic field. The ^{31}P ENDOR spectra were recorded using the Davies ENDOR ($\pi-\pi_{RF}-\pi/2-\tau-\pi-\tau-$echo),[36] and ^{13}C ENDOR spectra were recorded using Mims ENDOR ($\pi/2-\tau-\pi/2-\pi_{RF}-\pi/2-\tau-$echo)[37] pulse sequences, where the echo intensity is recorded as a function of the frequency of the RF π pulse. MW pulse durations were 12.5−17.5 ns for $\pi/2$ pulses in the Mims ENDOR sequence and 100 ns/200 ns for $\pi/2$, π pulses, respectively, in the Davies ENDOR sequence. The length of the RF pulses was 20−30 and 40 μs for the ^{31}P and ^{13}C ENDOR experiments, respectively. For the Mims ENDOR experiments, τ was set to 500 ns. For all ENDOR spectra, the magnetic field value was set to 3364 mT (maximum of the low-field line of the $|-1/2\rangle \rightarrow |1/2\rangle$ Mn^{2+} sextet), and the MW frequency was 94.9 GHz. The spectra were measured at 10 K with a repetition time of 1 ms[38] and 1 shot per point using the random acquisition protocol.[39] The experiment was repeated until the desired S/N ratio was achieved, and the accumulation time ranged from 3 to 24 h.

The frequency axes in the ^{31}P and ^{13}C ENDOR spectra are given with respect to the ^{31}P and ^{13}C Larmor frequencies, $\nu_{RF}-\nu_{31P}$, $\nu_{RF}-\nu_{13C}$, respectively. This allows one to directly read the hyperfine coupling from the spectrum. When the point dipole approximation applies, the principal components of the hyperfine coupling tensor are given by:

$$A_\perp = A_{iso} - T_\perp;\; A_\perp = A_{iso} + 2T_\perp \tag{1}$$

where A_{iso} is the isotropic component, and ($-T_\perp$, $-T_\perp$, 2 $T_\perp$) are the anisotropic principal components. $T_\perp$ is related to the electron−nuclear distance, r, according to:

$$r = \sqrt[3]{\frac{\mu_0}{4\pi}\frac{g_e g_n \beta_e \beta_n}{hT_\perp}} \tag{2}$$

All spectra were baseline corrected and normalized to the strongest signals (0:1) to ease the comparison in terms of frequency shifts. However, when the intensities of the ENDOR lines are of interest, then the ENDOR spectrum should be displayed according to the ENDOR effect:

$$\varepsilon = \frac{I(RF_{on}) - I(RF_{off})}{I(RF_{off})} \tag{3}$$

where $I(RF_{on})$ and $I(RF_{off})$ denote the echo intensity acquired with and without on-resonance RF irradiation, respectively.

Differences in the S/N ratio in the ENDOR spectra of different samples are due to variability in the sample concentrations and accumulation times.

RESULTS AND DISCUSSION

Twelve different complexes of the type (^{13}C)DbpA/Mn^{2+}/nucleotide/RNA, prepared with four types of nucleotides (ADP, ATP, ATPγS, and AMPPnP) in all possible combinations with dsRNA (double-stranded RNA), ssRNA (single-stranded RNA), and without RNA, were measured. The structures of the ATP analogs and the RNA constructs are shown in Figure 2. The minimal 33mer ssRNA construct, which is known to trigger DbpA ATP hydrolysis, consists of an HP92 hairpin followed by a 5′ extension.[10] The dsRNA construct was formed by annealing the ssRNA molecule with an 11mer RNA complementary to the 5′ extension. The double-stranded region of this dsRNA construct is too long to be efficiently unwound by DbpA.[13] We specifically chose a dsRNA that cannot be efficiently unwound, and therefore it can model the DbpA−RNA state prior to unwinding, whereas the complex with the ssRNA represents the state after unwinding.

The Mn^{2+} W-band echo-detected (ED) EPR spectra of all samples are similar, exhibiting six resolved ^{55} Mn hyperfine lines of the central $|-1/2, M_I\rangle \rightarrow |1/2, M_I\rangle$ transitions with a hyperfine splitting of 9 mT, superimposed on a broad background arising from all other transitions. Some typical spectra are shown in the Supporting Information (Figure S1). Small variations in the intensities and line-widths of the central transitions are attributed to the presence of free Mn^{2+}, the amount of which varied between different preparations. The observed changes were found to be within the experimental error, as concluded from a comparison of duplicates.

The local environment of the Mn^{2+} ion in all of the sample types investigated was explored through W-band (95 GHz) pulse ENDOR spectroscopy. Here, we focused on ^{31}P Davies ENDOR[36]

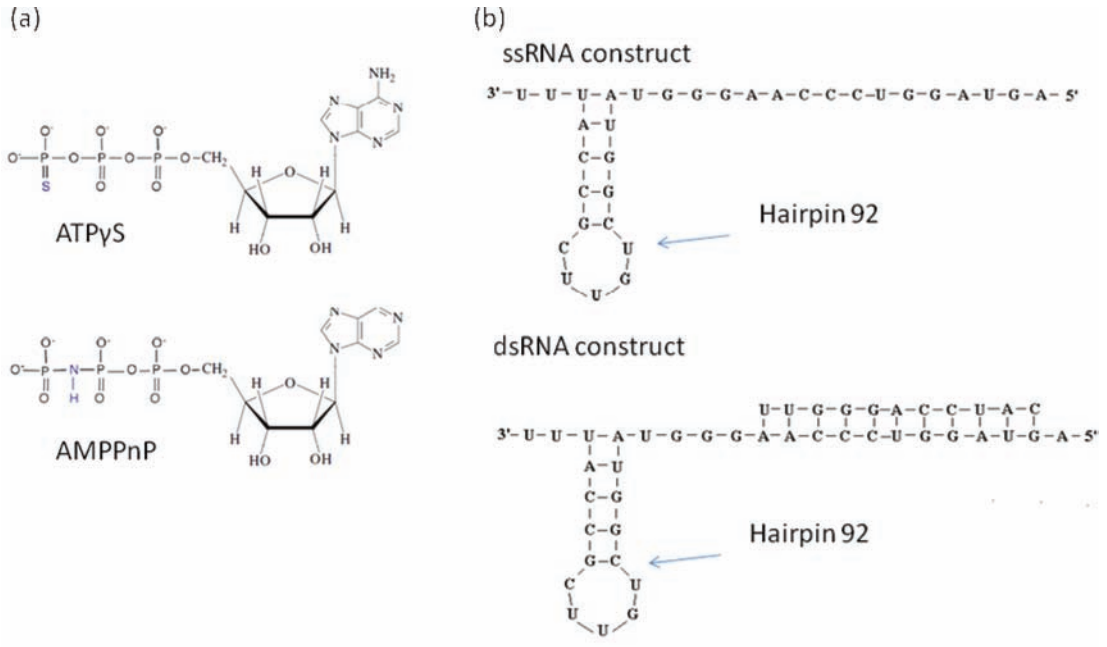

Figure 2. The nucleotides and the RNA constructs used in this work. (a) Structure of the ATP analogues ATPγS and AMPPnP, and (b) double-stranded (dsRNA) and single-stranded (ssRNA) constructs. The sequence of the ssRNA corresponds to the nucleotides 2531−2563 of 23S *E. coli* rRNA.

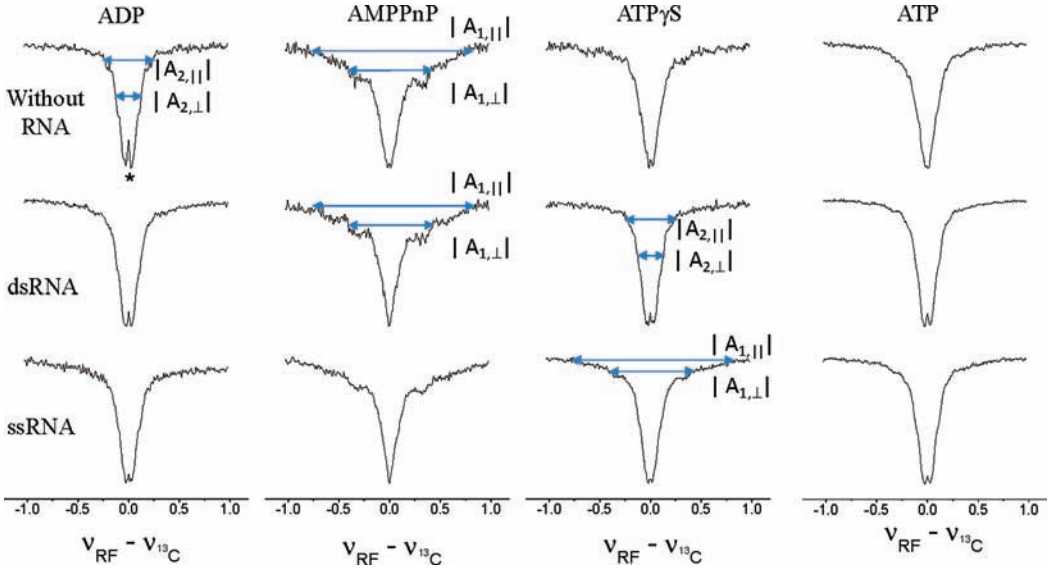

Figure 3. W-band Mims ^{13}C ENDOR spectra of the DbpA/RNA/Mn^{2+}/nucleotide complexes studied in this work, as labeled in the figure. All spectra are normalized to (0:1) and centered around $\nu(^{13}C)$ = 36.03 MHz. The resolved hyperfine couplings are denoted by arrows and marked in the figure.

for monitoring the coordination of Mn^{2+} to nucleotide phosphates and ^{13}C Mims ENDOR[37] for monitoring the coordination to DbpA.

The H_2O ligands of a Mn^{2+} ion have a well-defined and unique ^{1}H ENDOR spectrum.[40] Accordingly, ^{1}H ENDOR can be used to report on the presence of water ligands and, in principle, also on their number.[41,42] The determination of the number of bound water molecules relies on the intensity of the ENDOR effect. Indeed, we have observed ^{1}H signals that are typical of water ligands (see Figure S2, Supporting Information); however, due to the presence of $Mn(H_2O)_6^{2+}$ and unbound Mn^{2+}−nucleotide complexes in the samples, a quantitative analysis of the spectra in terms of the number of water ligands was not possible.

The Divalent Metal Cation Interaction with DbpA Residues. The ^{13}C Mims ENDOR spectra of the DbpA/Mn^{2+}/nucleotide/RNA complexes are shown in Figure 3. The presence of unbound Mn^{2+}/nucleotide complexes or RNA in the solution does not interfere with the ^{13}C ENDOR signals because the only source of these signals is bound DbpA. A common major feature in all 12 spectra is the relatively high intensity of the matrix line at the ^{13}C Larmor frequency, $\nu(^{13}C)$ = 36.03 MHz, arising from remote ^{13}C nuclei. Spectra with good S/N ratios also exhibit

Table 1. Summary of the Measured Hyperfine Parameters

sample	atom	$\lvert T_\perp \rvert$ (MHz)	$\lvert A_{iso} \rvert$ (MHz)	R (Å)	assignment
DbpA/Mn^{2+}/nucleotide/RNA	^{13}C	0.35 ± 0.1	0.85 ± 0.1	3.9 ± 0.3	C_β Thr 54
		or	or	or	or
		0.7 ± 0.1	0.1 ± 0.1	3.1 ± 0.3	C_β Thr 54 or C_δ Glu 154
DbpA/Mn^{2+}/ADP/RNA	^{13}C	0.25 ± 0.1	~ 0	4.3 ± 0.3	
DbpA/Mn^{2+}/ADP/RNA	^{31}P	0.75 ± 0.10	4.1 ± 0.1	3.52 ± 0.15	β-$^{31}PO_4$ ADP

several resolved shoulders on the wings of this line from ^{13}C nuclei that are close to Mn^{2+}. On the basis of comparison with earlier work on a relevant model system, $MnHCO_3^{(-)}$,[43] and on Mn^{2+} in the GTPase active site of Ras,[44] we assign these shoulders to hyperfine splittings of a single ^{13}C nucleus with $|A_{1,\parallel}|$ and $|A_{1,\perp}|$, as noted in Figure 3. These shoulders, although not as clear in all spectra, do have appreciable signal intensity in all of them, indicating the same binding mode of this ^{13}C nucleus in all samples.

There are two possible interpretations of $|A_{1,\parallel}|$ and $|A_{1,\perp}|$, depending on their relative signs. ENDOR simulations of the DbpA/Mn^{2+}/AMPPnP/ssRNA spectrum for the two options were carried out (Figure S3, Supporting Information). A simulation with opposite signs yielded $A_{iso} = 0.1 \pm 0.1$ MHz and $T_\perp = 0.7 \pm 0.1$ MHz. Using the point dipole approximation, which applies for a positive $T_\perp$ (see eq 1), we obtained a $Mn^{2+}-^{13}C$ distance of 3.1 ± 0.1 Å. The second possibility corresponds to $A_{1,\parallel}$ and $A_{1,\perp}$ having the same sign, and simulations for positive values yielded $A_{iso} = 0.85 \pm 0.1$ MHz, $T_\perp = 0.35 \pm 0.15$ MHz. Again, using the point-dipole approximation, this yields a $Mn^{2+}-^{13}C$ distance of 3.9 ± 0.3 Å. The two options differ in the signal intensity at the Larmor frequency region. Unfortunately, due to the presence of the strong matrix line, the simulations cannot be used to unambiguously determine the relative sign of the $A_\perp$ and $A_\parallel$, although the simulations with $|A_{1,\parallel}|$ and $|A_{1,\perp}|$ having the same sign show a somewhat better fit to the experimental spectrum. It is important to point out here that both interpretations of the ^{13}C ENDOR spectra reveal a direct binding of the amino acid residue to the Mn^{2+} ion most probably via an oxygen atom as discussed later. This is based on the short distance obtained for the first option and the appreciable A_{iso} for the second. In the derivation of the distances, we neglected any possibility of a significant spin densities on the bound oxygen and its coordinated ^{13}C because these are expected to be low and cause deviations of the anisotropic hyperfine interaction from axial symmetry that is well within our experimental error.[43]

We attempted to differentiate between the two options by recording a ^{13}C ENDOR spectrum at a magnetic field position just outside the central $|-1/2\rangle \rightarrow |1/2\rangle$ EPR transitions. There, the main contribution to the electron spin echo comes from the $|-3/2\rangle \rightarrow |-1/2\rangle$ EPR transitions. This ENDOR spectrum is then asymmetric with respect to the ^{13}C Larmor frequency and is dominated by nuclear transitions within the $M_s = -1/2$ and $-3/2$ manifolds. This allows one to determine the absolute sign of the hyperfine coupling.[40] The spectra obtained hinted toward the option of positive $A_{1,\parallel}$ and $A_{1,\perp}$, but because of the limited signal-to-noise (S/N) ratio and appearance of additional lines belonging to the $M_s = -3/2$ manifold of smaller ^{13}C hyperfine couplings, this assignment remained ambiguous. In addition, attempts to determine the sign of the hyperfine coupling by variable mixing time ENDOR[43,45] were unsuccessful due to S/N limitations.

Taking into account that an A_{iso} value of ~ 1 MHz was observed for $MnHCO_3^{(-)}$,[43] and $A_{iso} \approx 0.46$ MHz was reported for serine bound to Mn^{2+} in the GTP active site of Ras,[44] along with the indications provided by the simulations and the attempts to determine the sign of the hyperfine couplings described above, we prefer the option of the same signs that yield $A_{iso} = 0.85 \pm 0.1$ MHz and a $^{13}C-Mn^{2+}$ distance of 3.9 ± 0.3 Å, but we cannot exclude the second possibility, and therefore we listed both in Table 1.

A survey of crystal structures of related proteins (see the Supporting Information, Table S1) indicates that the most common amino acid residue coordinated to Mg^{2+} is the hydroxyl group of the conserved threonine of the Walker A motif. This corresponds to Thr 54 in DbpA. This residue is highly conserved across the SF1 and SF2 superfamilies,[4] and mutations of this residue abolish the ATPase activity of the enzymes.[46] The distance between Mg^{2+} and the β carbon of the conserved threonine in all crystal structures ranges from 3.05 to 3.86 Å (see Table S1). Another residue that was found to directly coordinate Mg^{2+} is the conserved glutamate, the second residue of the Walker B (DEAD/DExH) motif. The observed range of the $Mg^{2+}-\delta$ ^{13}C Glu distances is $3.05-3.11$ Å. On the basis of the above survey, the ^{13}C nucleus with $A_{1,\parallel}$ and $A_{1,\perp}$ is assigned to either the β carbon of Thr 54 or the δ carbon of Glu 154. In several crystal structures of DEAD-box proteins, the Mg^{2+} ion is bound to the protein through H-bonded water molecules and has no direct contact with any protein residue. We exclude this scenario for the DbpA active site arrangement because we observed a ^{13}C nucleus with either a significant isotropic contribution to the hyperfine interaction or a close distance to Mn^{2+} of ~ 3.1 Å in all DbpA/nucleotide complexes investigated, independent of the nucleotide type and the presence of RNA.

Interestingly, the ^{13}C $A_{1,\parallel}$ and $A_{1,\perp}$ signals exhibit the highest relative intensity in spectra of all of the AMPPnP complexes. Examination of the ENDOR effect (see eq 3) of the spectra shown in Figure 3 reveals that this intensity difference results from a weaker $\nu(^{13}C)$ line in the AMPPnP spectra. The shoulders appeared stronger in the spectra displayed in Figure 3 due to normalization according to the $\nu(^{13}C)$ line. Because the $\nu(^{13}C)$ line represents interaction with remote ^{13}C nuclei, this difference indicates changes in protein conformation around the Mn^{2+} ion for the AMPPnP complexes.

Another pair of resolved features is observed in the ^{13}C ENDOR spectra in all of the complexes except those with an AMPPnP nucleotide. These are denoted as $|A_{2,\parallel}|$ and $|A_{2,\perp}|$ in Figure 3. For these shoulders, we obtained $|A_{2,\parallel}| = 0.25 \pm 0.10$ MHz and $|A_{2,\perp}| = 0.5 \pm 0.1$ MHz, respectively, and calculated $A_{iso} \approx 0$, $T_\perp = 0.25 \pm 0.10$ MHz, and a $Mn^{2+}-^{13}C$ distance of 4.3 ± 0.3 Å, assuming the $A_{2,\parallel}$ and $A_{2,\perp}$ have opposite signs. The option of the same sign yields unrealistic values. This distance is more difficult to interpret, and it belongs either to a ^{13}C nucleus located farther away from the Mn^{2+} ion on the residue that directly coordinates Mn^{2+} or to a ^{13}C nucleus from a different residue that is spatially close. In the absence of a crystal structure, it is difficult to assign this distance to a specific atom or to a specific

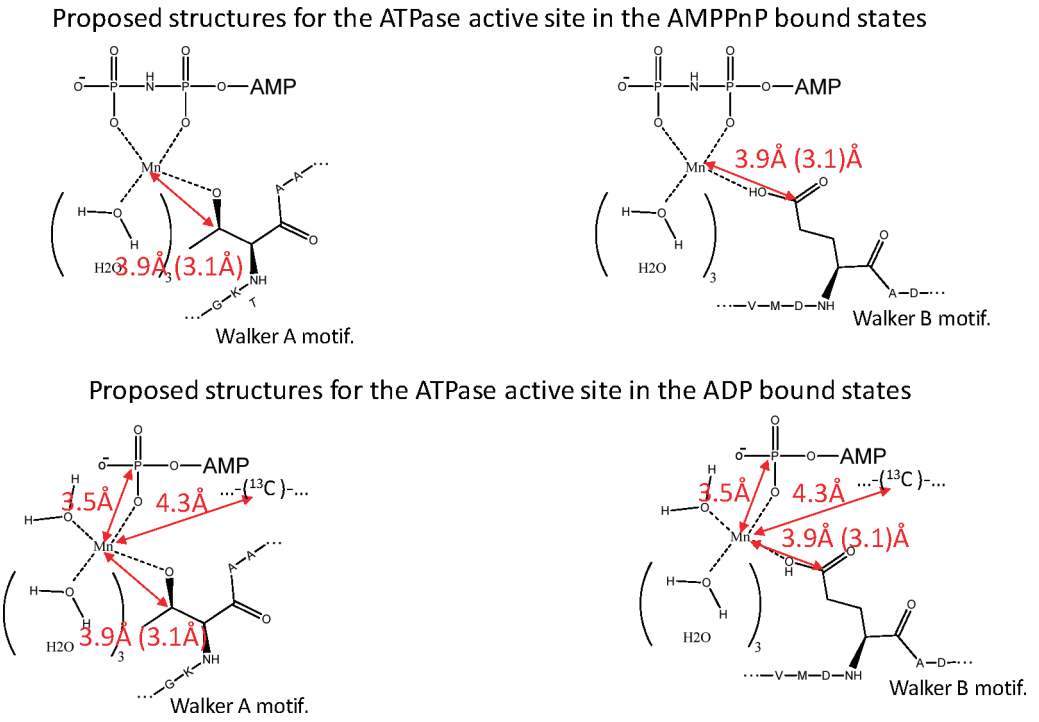

Figure 4. Schematic representation of the structure of the active site based on ENDOR-derived constraints. The number of water ligands was determined based on the assumption that Mn^{2+} is six coordinated. The two possible $Mn^{2+}-{}^{13}C$ distances found are noted.

amino acid residue. A schematic representation of the Mn^{2+} coordination in the active site, based on the above analysis, is illustrated in Figure 4. The measured ^{13}C hyperfine parameters are summarized in Table 1.

In the absence of its essential RNA cofactor, the ATP hydrolysis of DbpA occurs very slowly. This allowed us to observe the trapped, ATP-bound state. Prior to adding RNA to the DbpA/Mn^{2+}/nucleotide complex, three distinct types of ^{13}C ENDOR spectra were observed: the first for ATP and ATPγS, the second for AMPPnP, and the third for the ADP complexes (see Figure 3, first row and Figure S4). The main differences between the three types of spectra are in the overall shape of the $\nu(^{13}C)$ line, in the resolved $|A_{2,\parallel}|$ and $|A_{2,\perp}|$ features, and in the small splitting close to $\nu(^{13}C)$ (denoted by "*" in Figure 3 for the DbpA/Mn^{2+}/ADP complex). Most importantly, the spectra of DbpA with ATP and ATPγS significantly differ from the spectrum of the AMPPnP complex. This suggests that the protein part in the immediate vicinity of the Mn^{2+} cofactor in DbpA is sensitive to specific single atom substitutions in the vicinity of the γ phosphate in the bound nucleotide. It distinguishes AMPPnP from ATP, whereas it does not distinguish ATPγS from ATP

So far, we have detected differences in the Mn^{2+} binding site arising from different bound nucleotides. Next, we follow the effect of RNA binding. The width of the $\nu(^{13}C)$ line of the DbpA/Mn^{2+}/AMPPnP complex is larger than that of the DbpA/Mn^{2+}/AMPPnP/ssRNA and DbpA/Mn^{2+}/AMPPnP/dsRNA complexes (see Figure S5). The change in the $\nu(^{13}C)$ width indicates that some conformational changes took place in the vicinity (<6 Å) of the Mn^{2+} ion, but not in the residue that directly coordinates the ion. These structural changes may be responsible for the cooperative binding of Mg^{2+}/ATP and RNA reported earlier[47,48] and can be related to the closed conformation YxiN adopts upon simultaneous binding of RNA and AMPPnP.[22]

Comparison of the ^{13}C ENDOR spectra of DbpA/Mn^{2+}/ADP in the presence or absence of RNA did not reveal any differences, thus indicating that no significant rearrangement in the vicinity of the Mn^{2+} in the ATPase active site occurs upon RNA binding. The weak coupling between ADP and RNA binding was reported earlier.[48] This differs from the AMPPnP-bound state, as previously discussed.

Since it was proposed that the conserved glutamate from the DEAD motif activates the catalytic water molecule that attacks the γ phosphoryl group of ATP in homologous DEAD-box helicases,[23] DbpA Glu 154 is expected to undergo rearrangement upon addition of RNA, which promotes ATP hydrolysis. Because we have not observed any rearrangement in the first coordination shell of Mn^{2+} ion upon addition of RNA, it is tempting to speculate that the coordinating residue is Thr 54 rather than Glu 154 in the first place.

The ^{13}C ENDOR spectra of DbpA/Mn^{2+}/ATP with and without dsRNA differ, the former being similar to DbpA/Mn^{2+}/ADP and DbpA/Mn^{2+}/ADP/ds(ss)RNA (see Figure S6). The changes are small, and the main differences are in the width and line shape of the matrix line at ^{13}C Larmor frequency and the presence of the $A_{2,\parallel}$ and $A_{2,\perp}$ features. Because the relative changes are subtle, any conclusions based on these data alone would be ambiguous. However, because these observations are supported by the much more significant changes in the ^{31}P ENDOR spectra, discussed next, we can justify pointing out these differences here. We attribute these changes to ATP hydrolysis induced by RNA binding, generating the ADP-bound state of DbpA. Similar behavior is observed for ATPγS, which is presumably only slowly hydrolyzable; this will be discussed later. We did not detect any difference between the ^{13}C ENDOR spectra of the dsRNA and ssRNA complexes for all types of bound nucleotides.

To summarize, ^{13}C ENDOR was shown to be a sensitive tool that can reveal subtle changes in the conformations that the

dx.doi.org/10.1021/ja204291d |J. Am. Chem. Soc. 2011, 133, 15514–15523

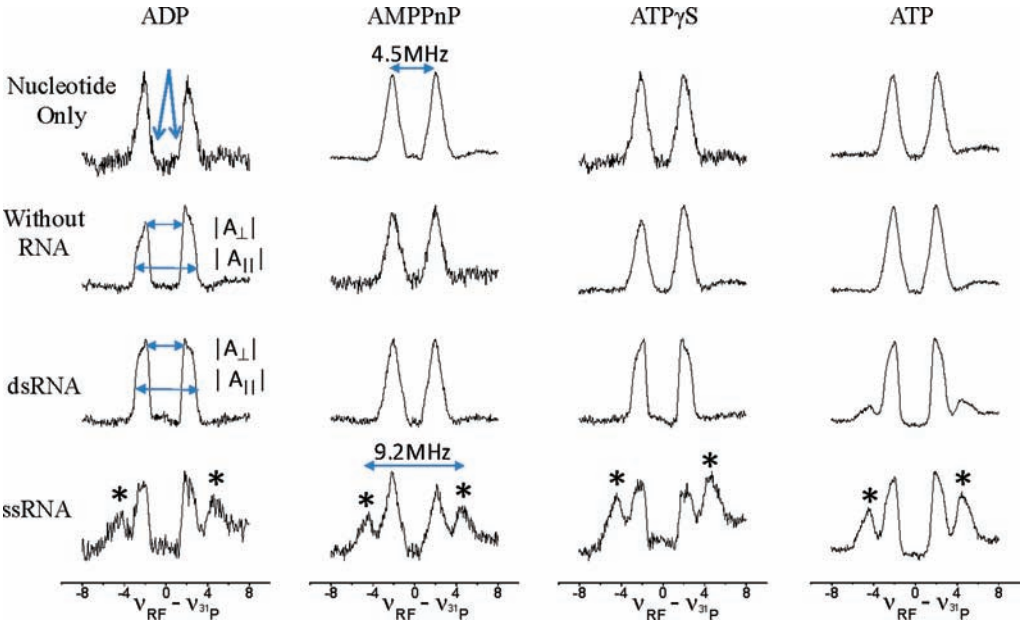

Figure 5. W-band Davies ^{31}P ENDOR spectra of the complexes studied in this work as labeled in the figure. All spectra are normalized to (0:1) and centered around $\nu(^{31}P)$ = 58.03 MHz. The resolved hyperfine couplings are denoted by arrows and marked in the figure.

ATPase active site adopts upon binding of various nucleotides. It provides quantitative data on the close protein coordination (first−third coordination shells) of the Mn^{2+} ion. Moreover, it reveals the coupling between RNA binding and conformational changes in the ATPase active site that occur not in the residue directly coordinating the Mn^{2+} metal cofactor but farther away.

The Divalent Metal Cation Interaction with the Nucleotides' Phosphates. The ^{31}P Davies ENDOR spectra of all samples under investigation display a doublet with an average splitting of 4.5 MHz centered at the ^{31}P Larmour frequency, $\nu(^{31}P)$ = 58.03 MHz (Figure 5). The spectra differ in the details of the line shape of this doublet.

In the first row of Figure 5, we present ^{31}P ENDOR spectra for the Mn^{2+}/nucleotide complexes without DbpA and without RNA. ^{31}P ENDOR spectra of the ADP/Mn^{2+} and ATPγS/Mn^{2+} complexes were reported and analyzed in a previous publication.[49] It was found that in the ATPγS/Mn^{2+} complex the nucleotide is bound to Mn^{2+} with two phosphates directly coordinating the ion. We extend this conclusion to AMPPnP/Mn^{2+} and ATP/Mn^{2+} because all three complexes have virtually identical spectra. The gradual slope toward the center of the spectrum (see Figure S7) was attributed to the presence of two magnetically inequivalent ^{31}P nuclei with slightly different hyperfine couplings.[49] These spectra have symmetric-looking line shapes, and we will refer hereafter to this type of spectra as ATP-type spectra. The line shape of the Mn^{2+}/ADP complex has a sharp edge toward the center of the doublet (see the arrows in Figure 5 for the ADP/Mn^{2+} spectrum and Figure S7), whereas for the ATP-type spectrum the edge is more gradual.

The second row of Figure 5 presents spectra of the DbpA/Mn^{2+}/nucleotide complexes without RNA. The spectra of DbpA/Mn^{2+}/ATPγS, AMPPnP, and ATP are generally similar to the corresponding spectra of the Mn^{2+}/nucleotides without DbpA, shown in the top row of Figure 5. This shows that the mode of Mn^{2+} binding to ATP and its analogs does not change upon binding to DbpA in the absence of RNA. On the basis of the available crystal structures of the DEAD proteins cocrystallized with AMPPnP,[23−26,50,51] we can conclude that in the ATP, ATPγS, and AMPPnP complexes with DbpA, Mn^{2+} is coordinated by the β and γ phosphates.

The line shape of the DbpA/Mn^{2+}/ADP spectrum (Figure 5, second row) is significantly different from that of the spectrum of Mn^{2+}/ADP alone (Figure 5, first row). With DbpA, the $A_{||}$ and $A_{\perp}$ singularities become resolved and yield $|A_{||}| = 5.6 \pm 0.1$ MHz and $|A_{\perp}| = 3.3 \pm 0.1$ MHz, as indicated in Figure 5. From these, we derived $|A_{iso}| = 4.1 \pm 0.1$ MHz and $|T_{\perp}| = 0.75 \pm 0.10$ MHz, and a $Mn^{2+}-{}^{31}P$ distance of 3.52 ± 0.15 Å. This is in close agreement with the $Mg^{2+}-{}^{31}P$ (β ADP) distances observed in the crystal structures of the DEAD proteins cocrystallized with Mg^{2+}/ADP (see Table S1 and references therein.)

The spectra with the sharp edge toward the doublet center and the resolved powder pattern singularities will be referred to hereafter as ADP-type spectra. ADP-type spectra therefore represent a significant rearrangement of the ADP/Mn^{2+} complex upon binding to DbpA, with only one phosphate directly coordinating the Mn^{2+} ion, as opposed to two phosphates in free Mn^{2+}/ADP.[49,52] The above ^{31}P ENDOR data establish W-band ^{31}P ENDOR as a sensitive method that can distinguish between the ADP and ATP-bound states of DbpA. It complements the ^{13}C ENDOR sensitivity to Mn^{2+} interaction with the protein interactions in different states. The Mn^{2+} phosphate coordination for the DbpA-bound states is schematically illustrated in Figure 4 for the ADP- and AMPPnP-bound complexes.

The third row of Figure 5 presents the spectra of the DbpA/Mn^{2+}/nucleotide/dsRNA complexes. The spectra of DbpA/Mn^{2+}/ADP/dsRNA and DbpA/Mn^{2+}/AMPPnP/dsRNA retain the respective spectral features of those complexes without dsRNA. (Compare the third and second rows in Figure 5.) Because the shape of the 4.5 MHz doublet of all of the ADP- and AMPPnP-bound complexes does not change upon the addition of dsRNA, we can conclude that no significant changes in the nucleotide phosphate coordination occur upon binding of dsRNA.

DbpA Hydrolyzes ATPγS in the Presence of dsRNA. In contrast to DbpA/Mn^{2+}/ADP and DbpA/Mn^{2+}/AMPPnP,

which do not exhibit any significant change in the ^{31}P spectrum upon dsRNA binding, the DbpA/Mn^{2+}/ATP/complex switched from the ATP-type in the complex without dsRNA to the ADP-type spectrum in the presence of dsRNA. This is expected if ATP is hydrolyzed. An additional doublet with a 9.2 MHz splitting that appears in this spectrum is attributed to the small amount of ssRNA present in this preparation; the source of this signal is discussed next. Similar changes in the line shapes of the ENDOR spectra were also observed for ATPγS. These changes are in line with our earlier observations that in the presence of dsRNA, the ^{13}C spectra of DbpA/Mn^{2+}/ATPγS/become similar to those of the analogous ADP complexes (Figure 3). (Similar spectral changes were also observed for ssRNA.) This suggests that DbpA, which is known to hydrolyze ATP only in the presence of the specific RNA that contains the HP92 sequence,[10] is able to efficiently hydrolyze ATPγS as well.

The line shape of the 4.5 MHz ^{31}P doublet in the spectra of DbpA/Mn^{2+}/nucleotide/ssRNA complexes, shown in row 4 of Figure 5, is similar to that observed for the respective dsRNA complexes. The complexes with ADP and AMPPnP nucleotides retained their respective spectral features of the complexes without ssRNA (apart from the additional 9.2 MHz doublet), whereas the ATPγS and ATP complexes switched to an ADP-type spectrum. We therefore can conclude that ATPγS hydrolysis occurs efficiently with both ssRNA and dsRNA constructs, which is expected because both constructs contain the HP92 sequence.

We want to stress here that the above conclusion was based solely on the analysis of the ENDOR spectroscopic data. We then confirmed this observation independently by following ATPγS hydrolysis using ^{35}S-labeled Mg^{2+}/ATPγS. (See the Supporting Information, Figure S9.) ATPγS is therefore not a good ATP analogue for structural studies of DbpA/RNA. It was employed in an earlier study of DbpA as a slowly hydrolyzable ATP analogue,[21] but in that specific study the RNA cofactor used was different from the one known to activate the DbpA ATPase activity, which may account for the lack of rapid ATPγS hydrolysis. The inability of DbpA to distinguish between the ATPγS and ATP nucleotides suggests that either the interaction of the protein with the γ phosphate of ATP is not sensitive to the sulfur substitution, or, more likely, that not all terminal oxygen atoms of the γ phosphate form ATPase important interactions with protein residues, therefore resulting in a lack of discrimination between ATPγS and ATP. Efficient hydrolysis of ATPγS was reported for another DEAD-box protein, eIF4A.[53] Our observation suggests that this reported activity may be general for the DEAD-box family of RNA helicases.

High-Affinity Mn^{2+} Binding Site in ssRNA. The results of the ^{31}P ENDOR measurements with ssRNA are depicted in the fourth row of Figure 5. In all complexes with ssRNA, an additional doublet with an average splitting of 9.2 MHz, denoted by "*" in Figure 5, appears. This doublet is assigned to ^{31}P nuclei of the ssRNA phosphate backbone. We attribute the appearance of this doublet to the formation of a high-affinity Mn^{2+} binding site somewhere in the 5′ extension of the ssRNA construct, which competes with the ATPase active site for Mn^{2+} binding. The ^{31}P ENDOR spectrum of Mn^{2+}/ADP/ssRNA without DbpA exhibits the same doublet of 9.2 MHz (see Figure S8), thus confirming that it is unique to ssRNA and that it does not involve DbpA. This hyperfine coupling is close to that reported for the high-affinity Mn^{2+} site in the hammerhead ribozyme ($A_{31P} \approx 8.5 \pm 0.5$ MHz).[54] The proposed formation of the high-affinity pocket is illustrated in Figure 6a. The relative intensity of 4.5 and 9.2 MHz doublets shows that the Mn^{2+} binding site in ssRNA has a binding affinity comparable to that of free or DbpA-bound nucleotides.

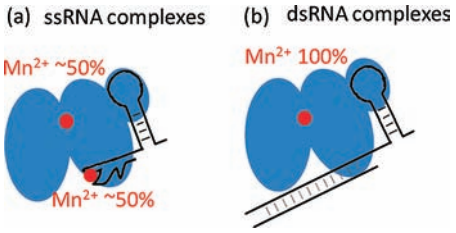

Figure 6. Schemes illustrating (a) the formation of the high-affinity binding site in the 5′ extension of the DbpA, which competes with the ATPase active site for Mn^{2+} binding. (b) Mn^{2+} high-affinity binding site is no longer formed in the 5′ extension of the RNA molecule due to Watson−Crick base pairing with 11mer complementary RNA.

The 9.2 MHz doublet is absent from the ^{31}P ENDOR spectra of the DbpA/Mn^{2+}/nucleotide/dsRNA complexes previously discussed (Figure 5, third row), indicating that the affinity of dsRNA to Mn^{2+} is considerably smaller than that of ssRNA. This is attributed to 5′ extension of 33mer RNA adopting a different conformation due to the Watson Crick base pairing with an 11mer complementary RNA, as illustrated in Figure 6b. The weak intensity of the 9.2 MHz doublet in the DbpA/Mn^{2+}/ATP/dsRNA spectrum is attributed to small amounts of ssRNA present in that preparation.

Importantly, ^{31}P ENDOR spectroscopy is able to monitor the migration of Mn^{2+} to the RNA molecule in the ssRNA constructs. Mn^{2+} is used as a probe for different types of spectroscopic measurements, such as EXAFS, which usually cannot distinguish different binding sites. The EXAFS data are fitted to a model of a priori-assumed binding site with many variable parameters. Therefore, a prior confirmation of the exact localization of the probe at the target site (the ATPase active site in our case) that can be supplied by ENDOR is crucial for the structural analysis. Further studies are required to completely characterize the Mn^{2+} binding site in ssRNA. Of particular interest may be the use of the 9.2 MHz ^{31}P doublet to probe RNA unwinding for shorter dsRNAs. For this to occur, the corresponding kinetics for the Mn^{2+} binding must be fast enough.

General Mechanistic Implications. The overall positioning of ATP/Mn^{2+} in the DbpA pocket is governed by multiple interactions between the protein and the nucleotide/Mn^{2+} complex. In all of the observed states of the active site, the Mn^{2+} cofactor was found to coordinate a single DbpA residue. This indicates that the positioning of the nucleotide/Mn^{2+} in the DbpA active site is governed mainly by the interactions of the nucleotide sugar, phosphate and base moieties with the protein. With three and four water ligands in the ATP- and ADP-bound states, respectively, the Mn^{2+} metal cofactor is prone to ligand exchange throughout the catalytic cycle.

RNA with a HP92 structure is known to activate ATP hydrolysis of DbpA. Binding of the RNA molecule should therefore promote changes in the protein in the vicinity of γ phosphate of the ATP. The most probable candidate for activating the ATP hydrolysis is a correctly positioned glutamate residue of the DEAD motif.[23] Amino acids surrounding the γ phosphate adopt specific positions upon binding of RNA, which in turn places the ATP nucleotide in the correct spatial conformation suitable for hydrolysis. Interestingly, prior to adding the RNA molecule, the state that DbpA adopts is different for AMPPnP and ATP, with ATPγS being similar to the ATP state. Upon addition of RNA,

ATP, and ATPγS, but not AMPPnP, nucleotides undergo rapid hydrolysis by DbpA.

Importantly, whereas DbpA can hydrolyze ATPγS, it still does not promote RNA unwinding of RNA.[15] It can be speculated that a one-atom change in the leaving phosphate group may interfere with the cascade of events needed for disruption of dsRNA. The two arginines (331, 334) of motif VI were proposed to discriminate between the ADP- and ATP-bound forms of the DEAD-box helicases.[23] The absence of RNA unwinding with ATPγS nucleotide suggests that some important interaction with one or both residues is disrupted due to the presence of the thio group. Perhaps the hydrogen bond, which normally involves an oxygen atom, is not strong enough when the sulfur atom substitutes for the oxygen. This weaker bond is in turn insufficient to trigger the sequence of events that normally occurs after ATP hydrolysis.

According to the proposed mode of action for DEAD-box helicases, the strand separation event is coupled to the formation of the ATP or ADP-Pi bound, tense from, that disrupts the double-stranded RNA structure. The release of ADP-Pi is then only needed for enzyme recycling during multiple turnovers.[15,55,56] Accordingly, a good ATP or ADP-Pi analogie would promote the strand separation as well, by correctly mimicking the tense ADP-Pi state. AMPPnP does not promote RNA remodeling in any of the investigated systems.[55,57] It is therefore unclear what type of intermediate in the ATP-dependent RNA unwinding process is trapped by AMPPnP. We provide experimental evidence that AMPPnP is indeed positioned in a different manner as compared to ATP and ATPγS in the active site of DbpA even prior to RNA binding. The structure of the active site for the two nucleotides differs in the arrangement of the DbpA side chains around the bound Mn^{2+}/nucleotide. ATP and ATPγS are initially positioned in a proper way to undergo hydrolysis; this is supported by the ^{13}C ENDOR spectra of the DbpA/Mn^{2+}/ATPγS complex resembling more the DbpA/Mn^{2+}/ADP spectra than the DbpA/Mn^{2+}/AMPPnP spectra. Although the Mn^{2+} coordination by nucleotide phosphates is similar for ATP, ATPγS, and AMPPnP, the protein states are different as is evident from the ^{13}C spectra. The nitrogen atom in P−NH−P is a hydrogen-bond donor as opposed to oxygen in the P−O−P, which is a hydrogen-bond acceptor. This may partially account for the ATPase active site adopting distinct conformations in the ATP/ATPγS- and AMPPnP-bound states.

Finally, we did not observe significant changes in the first coordination shell of Mn^{2+} upon binding of RNA in both the AMPPnP and the ADP states. Changes are detected for AMPPnP in shells farther away. We therefore suggest that the fine changes that occur in the active site of the protein upon binding of RNA occur mostly in the vicinity of the γ phosphate, as previously discussed. Nevertheless, this does not exclude the possibility that changes in the direct coordination of the Mn^{2+} cofactor occur during catalysis.

CONCLUSIONS

The close environment of the Mn^{2+} ion at the ATPase active site in various states of DbpA, which are highly relevant to understanding of its mode of action, was probed by W-band ENDOR spectroscopy. Specifically, our findings are as follows:

(1) The Mn^{2+} ion is coordinated to a single amino acid in all of the investigated states of DbpA. This residue is assigned to either Thr54 in the Walker A motif or Glu154 in the Walker B (DEAD) motif.

(2) Three different conformations of the ATPase active site of DbpA prior to RNA binding were observed, the first with AMPPnP, the second with ADP, and the last with hydrolyzable ATPγS and ATP.

(3) The ATPase active site of DbpA cannot efficiently differentiate between ATP and ATPγS, and both are efficiently hydrolyzed in the presence of the RNA substrate that contains the HP92 sequence.

(4) The first and second coordination shells of the Mn^{2+} ion in the AMPPnP/DbpA complexes are not affected by the binding of the RNA substrates used in this study. However, changes in more distant shells do take place. Such structural changes were not detected for the ADP state.

(5) We observed a migration of approximately 50% of the Mn^{2+} ions to a high-affinity binding site formed in the 5′ extension of the ssRNA construct. This site is not formed in the 5′ extension of the dsRNA construct due to the Watson Crick base pairing with 11mer complementary RNA.

We showed that Mn^{2+} substitution for Mg^{2+}, together with high-field ENDOR spectroscopy, is an efficient tool for molecular level (angstrom scale) investigation of the ATPase active site of DEAD-box helicase. This study of the various trapped states of DbpA/nucleotide/Mn^{2+}/RNA paves the way for time-resolved studies where the transition from state to state can be monitored.

ASSOCIATED CONTENT

Supporting Information. Table with a summary of the observed Mg^{2+} coordination in the available crystal structures of DEAD-box helicases, ^{1}H ENDOR, ^{13}C ENDOR simulations, echo detected EPR spectra of selected complexes, comparison of ENDOR spectra, ^{31}P ENDOR of the Mn^{2+}/ADP/ssRNA mixture, and ATPγS hydrolysis measurements. This material is available free of charge via the Internet at http://pubs.acs.org.

AUTHOR INFORMATION

Corresponding Author
daniella.goldfarb@weizmann.ac.il

ACKNOWLEDGMENT

All molecular biology work was performed at the NanoBio center of chemical research support, WIS; we thank Dr. Yoav Barak for his guidance and advice. We thank Dr. Arnon Henn for useful discussions and comments on this work. We thank Dr. Shira Albeck and Dr. Yoav Peleg from the Israel Structural Proteomics Center for their help with purification of the ^{13}C-labeled DbpA samples. We thank Dr. Eyal Kamhi and Prof. Joseph Sperling for their assistance and guidance regarding RNA handling. We thank Adi Moseri for his help with overexpression of ^{13}C-labeled DbpA samples. This research was supported by the Israel Science Foundation (ISF). D.G. holds the Erich Klieger Professorial Chair in Chemical Physics.

REFERENCES

(1) Iost, I.; Dreyfus, M. *Nucleic Acids Res.* **2006**, *34*, 4189–4197.
(2) Pyle, A. M. *Annu. Rev. Biophys.* **2008**, *37*, 317–336.
(3) Anantharaman, V.; Koonin, E. V.; Aravind, L. *Nucleic Acids Res.* **2002**, *30*, 1427–1464.
(4) Fairman-Williams, M. E.; Guenther, U.-P.; Jankowsky, E. *Curr. Opin. Struct. Biol.* **2010**, *20*, 313–324.

(5) Walker, J. E.; Saraste, M.; Runswick, M. J.; Gay, N. J. *EMBO J.* **1982**, *1*, 945–951.
(6) Bleichert, F.; Baserga, S. J. *Mol. Cell* **2007**, *27*, 339–352.
(7) Cordin, O.; Banroques, J.; Tanner, N. K.; Linder, P. *Gene* **2006**, *367*, 17–37.
(8) Peil, L.; Virumäe, K.; Remme, J. *FEBS J.* **2008**, *275*, 3772–3782.
(9) Hilbert, M.; Karow, A. R.; Klostermeier, D. *Biol. Chem.* **2009**, *390*, 1237–1250.
(10) Tsu, C. A.; Kossen, K.; Uhlenbeck, O. C. *RNA* **2001**, *7*, 702–709.
(11) Kossen, K.; Uhlenbeck, O. C. *Nucleic Acids Res.* **1999**, *27*, 3811–3820.
(12) Fuller-Pace, F. V.; Nicol, S. M.; Reid, A. D.; Lane, D. P. *EMBO J.* **1993**, *12*, 3619–3626.
(13) Diges, C. M.; Uhlenbeck, O. C. *EMBO J.* **2001**, *20*, 5503–5512.
(14) Henn, A.; Medalia, O.; Shi, S. P.; Steinberg, M.; Franceschi, F.; Sagi, I. *Proc. Natl. Acad. Sci. U.S.A.* **2001**, *98*, 5007–5012.
(15) Henn, A.; Cao, W.; Licciardello, N.; Heitkamp, S. E.; Hackney, D. D.; De La Cruz, E. M. *Proc. Natl. Acad. Sci. U.S.A.* **2010**, *107*, 4046–4050.
(16) Karginov, F. V.; Caruthers, J. M.; Hu, Y.; McKay, D. B.; Uhlenbeck, O. C. *J. Biol. Chem.* **2005**, *280*, 35499–35505.
(17) Kossen, K.; Karginov, F. V.; Uhlenbeck, O. C. *J. Mol. Biol.* **2002**, *324*, 625–636.
(18) Hardin, J. W.; Hu, Y. X.; McKay, D. B. *J. Mol. Biol.* **2010**, *402*, 412–427.
(19) Wang, S.; Overgaard, M. T.; Hu, Y.; McKay, D. B. *Biophys. J.* **2008**, *94*, L01–L03.
(20) Karow, A. R.; Klostermeier, D. *J. Mol. Biol.* **2010**, *402*, 629–637.
(21) Henn, A.; Shi, S.-P.; Zarivach, R.; Ben-Zeev, E.; Sagi, I. *J. Biol. Chem.* **2002**, *277*, 46559–46565.
(22) Theissen, B.; Karow, A. R.; Köhler, J.; Gubaev, A.; Klostermeier, D. *Proc. Natl. Acad. Sci. U.S.A.* **2008**, *105*, 548.
(23) Sengoku, T.; Nureki, O.; Nakamura, A.; Kobayashi, S.; Yokoyama, S. *Cell* **2006**, *125*, 287–300.
(24) Andersen, C. B. F.; Ballut, L.; Johansen, J. S.; Chamieh, H.; Nielsen, K. H.; Oliveira, C. L. P.; Pedersen, J. S.; Seraphin, B.; Hir, H. L.; Andersen, G. R. *Science* **2006**, *313*, 1968–1972.
(25) Bono, F.; Ebert, J.; Lorentzen, E.; Conti, E. *Cell* **2006**, *126*, 713–725.
(26) Del Campo, M.; Lambowitz, A. M. *Mol. Cell* **2009**, *35*, 598–609.
(27) Pause, A.; Méthot, N.; Svitkin, Y.; Merrick, W. C.; Sonenberg, N. *EMBO J.* **1994**, *13*, 1205–1215.
(28) Pause, A.; Méthot, N.; Sonenberg, N. *Mol. Cell. Biol.* **1993**, *13*, 6789–6798.
(29) Scheffzek, K.; Ahmadian, M. R.; Kabsch, W.; Wiesmüller, L.; Lautwein, A.; Schmitz, F.; Wittinghofer, A. *Science* **1997**, *277*, 333–339.
(30) Zoleo, A.; Lippe, G.; Contessi, S.; Brustolon, M.; Dabbeni-Sala, F.; Maniero, A. L. *Biochemistry* **2007**, *46*, 13443–13450.
(31) Reed, G. H.; Poyner, R. R. *Met. Ions Biol. Syst.* **2000**, *37*, 183–207.
(32) Akabayov, B. Structural dynamic insights into the selective catalysis of the RNA helicase DbpA. Ph.D. Thesis, Weizmann Institute of Science, 2007.
(33) Möbius, K.; Goldfarb, D. *Adv. Photosynth. Respir.* **2008**, *26*, 267–304.
(34) Goldfarb, D.; Lipkin, Y.; Potapov, A.; Gorodetsky, Y.; Epel, B.; Raitsimring, A. M.; Radoul, M.; Kaminker, I. *J. Magn. Reson.* **2008**, *194*, 8–15.
(35) Gromov, I.; Krymov, V.; Manikandan, P.; Arieli, D.; Goldfarb, D. *J. Magn. Reson.* **1999**, *139*, 8–17.
(36) Davies, E. R. *Phys. Lett. A* **1974**, *47*, 1–2.
(37) Mims, W. B. *Proc. R. Soc. London, Ser. A* **1965**, *283*, 452–457.
(38) For some of the ENDOR spectra, the actual repetition time was ~12−14 ms due to the delay introduced by data transfer from the NI6013 ADC card to the software. This delay is absent on the current configuration of the spectrometer that uses the Acqiris DP310 digitizer (Agilent Technologies) for data acquisition.
(39) Epel, B.; Arieli, D.; Baute, D.; Goldfarb, D. *J. Magn. Reson.* **2003**, *164*, 78–83.
(40) Manikandan, P.; Carmieli, R.; Shane, T.; Kalb (Gilboa), J.; Goldfarb, D. *J. Am. Chem. Soc.* **2000**, *122*, 3488–3494.
(41) Raitsimring, A. M.; Astashkin, A. V.; Baute, D.; Goldfarb, D.; Poluektov, O. G.; Lowe, M. P.; Zech, S. G.; Caravan, P. *ChemPhysChem* **2006**, *7*, 1590–1597.
(42) Zech, S. G.; Sun, W.; Jacques, V.; Caravan, P.; Astashkin, A. V.; Raitsimring, A. M. *ChemPhysChem* **2005**, *6*, 2570–2577.
(43) Potapov, A.; Goldfarb, D. *Inorg. Chem.* **2008**, *47*, 10491–10498.
(44) Bennati, M.; Hertel, M. M.; Fritscher, J.; Prisner, T. F.; Weiden, N.; Hofweber, R.; Spörner, M.; Horn, G.; Kalbitzer, H. R. *Biochemistry* **2006**, *45*, 42–50.
(45) Epel, B.; Pöppl, A.; Manikandan, P.; Vega, S.; Goldfarb, D. *J. Magn. Reson.* **2001**, *148*, 388–397.
(46) Hishida, T.; Iwasaki, H.; Yagi, T.; Shinagawa, H. *J. Biol. Chem.* **1999**, *274*, 25335–25342.
(47) Polach, K. J.; Uhlenbeck, O. C. *Biochemistry* **2002**, *41*, 3693–3702.
(48) Henn, A.; Cao, W.; Hackney, D. D.; De La Cruz, E. M. *J. Mol. Biol.* **2008**, *377*, 193–205.
(49) Potapov, A.; Goldfarb, D. *Appl. Magn. Reson.* **2006**, *30*, 461–472.
(50) von Moeller, H.; Basquin, C.; Conti, E. *Nat. Struct. Mol. Biol.* **2009**, *16*, 247–254.
(51) Collins, R.; Karlberg, T.; Lehtiö, L.; Schütz, P.; van den Berg, S.; Dahlgren, L.-G.; Hammarström, M.; Weigelt, J.; Schüler, H. *J. Biol. Chem.* **2009**, *284*, 10296–10300.
(52) For the DbpA/ADP/Mn^{2+} preparation, we expect ~30% of the unbound ADP/Mn^{2+} to be free in solution, which accounts for the ENDOR line shapes diverging from the clean powder pattern line shapes.
(53) Peck, M. L.; Hershlag, D. *RNA* **2003**, *9*, 1180–1187.
(54) Schiemann, O.; Carmieli, R.; Goldfarb, D. *Appl. Magn. Reson.* **2007**, *31*, 543–552.
(55) Liu, F.; Putnam, A.; Jankowsky, E. *Proc. Natl. Acad. Sci. U.S.A.* **2008**, *105*, 20209–20214.
(56) Chen, Y.; Potratz, J. P.; Tijerina, P.; Del Campo, M.; Lambowitz, A. M.; Russell, R. *Proc. Natl. Acad. Sci. U.S.A.* **2008**, *105*, 20203–20208.
(57) Yang, Q.; Jankowsky, E. *Nat. Struct. Mol. Biol.* **2006**, *13*, 981–986.